Forschungszentrum Karlsruhe

Technik und Umwelt

Wissenschaftliche Berichte

FZKA 6603

Neutrino Flux Calculations for the Tungsten Target of the ISIS Spallation Neutron Facility

P. Plischke and R. L. Burman*

Institut für Kernphysik

* *Permanent address: P-Division, Los Alamos National Laboratory, Los Alamos, New Mexico 87545, USA.*

Forschungszentrum Karlsruhe GmbH, Karlsruhe

2001

Impressum der Print-Ausgabe:

Als Manuskript gedruckt
Für diesen Bericht behalten wir uns alle Rechte vor

Forschungszentrum Karlsruhe GmbH
Postfach 3640, 76021 Karlsruhe

Mitglied der Hermann von Helmholtz-Gemeinschaft
Deutscher Forschungszentren (HGF)

ISSN 0947-8620

Abstract

The neutrino flux produced by the spallation neutron source ISIS at the position of the KARMEN neutrino experiment, for a new tungsten spallation target, is calculated to an accuracy of 6.7%. Contributions from the spallation and μSR targets to the ν_μ, ν_e, and $\overline{\nu}_\mu$ fluxes, due to π^+ and μ^+ decay at rest, are evaluated. Results are presented in terms of neutrinos per proton for an incident proton beam of 800 MeV. The contamination of $\bar{\nu}_e$, from the π^- decay-in-flight and μ^- decay-at-rest chain, is found to be 0.034% with an accuracy of 12%. Comparisons are made of the measured and calculated values of a variety of neutrino induced reactions; agreement for the absolute cross sections implies that the calculated neutrino fluxes used were reasonably accurate.

Berechnung der Neutrinoflüsse für das Wolfram-Target an der ISIS Spallationsneutronenquelle

Zusammenfassung

Der Fluß von Neutrinos von der Spallationsneutronenquelle ISIS am Ort des Neutrino-Experiments KARMEN wird berechnet mit einer Genauigkeit von 6.7% für das neue Wolfram-Target. Beiträge des Spallations- und des μSR- Targets zu den Flüssen von ν_μ, ν_e und $\overline{\nu}_\mu$ aus dem π^+ und μ^+ Zerfall in Ruhe werden bestimmt. Die Ergebnisse werden dargestellt als Neutrinos pro Proton für eine Protonen-Energie von 800 MeV. Der störende Anteil an $\bar{\nu}_e$ aus dem π^- Zerfall im Fluge und anschließendem μ^- Zerfall in Ruhe wird zu 0.034% bestimmt mit einer Genauigkeit von 12%. Messungen einiger Neutrino-Wirkungsquerschnitte werden mit theoretischen Rechnungen verglichen. Die gute Übereinstimmung der absoluten Werte zeigt, dass die dabei verwendeten berechneten Neutrino-Flüsse vernünftige Werte haben.

---

1 Introduction

The ISIS facility at the Rutherford Appleton Laboratory in Oxfordshire, UK, is a pulsed neutron source intended primarily for condensed matter studies. Besides neutrons, the facility produces in its spallation target a large number of pions; the charged pions eventually stop and produce intense neutrino beams. These neutrino beams have been used for an extensive program of neutrino research at the KARMEN neutrino experiment[1], operated by a collaboration of the Forschungszentrum Karlsruhe, University of Karlsruhe, University of Bonn, University Erlangen-Nürnberg, Rutherford Appleton Laboratory, Queen Mary and Westfield College, London and Oxford University.

ISIS is based upon an 800 MeV rapid-cycling (50 Hz) proton synchrotron with a design beam intensity of 200 μA. This pulsed proton beam is used to produce fluxes of pulsed neutrons in heavy metallic targets. To date, the protons have been dumped in a massive tantalum or uranium target, producing neutrons from spallation and fission processes [2]. Several improvement projects are now being considered for the ISIS facility: theseinclude a new spallation target, and a 50% increase in the proton beam intensity to 300 μA. The new spallation target, composed primarily of tungsten, is likely to be installed sometime in 2001.

This report presents a calculation of the neutrino fluxes to be expected from the new tungsten spallation target. Previous publications [3] have given the results of calculations of neutrino fluxes for the existing tantalum and uranium targets. A Monte Carlo code for pion production and pion and muon tracking was developed[4] for the simulation of neutrinos from π^+ and μ^+ decay at rest; the extension of that code to the production, tracking, and decay of π^- and μ^- is given in ref. [3]. This computer code has been widely used for neutrino experiments at ISIS and at the Los Alamos National Laboratory (LAMPF; now LANSCE). Since extensive documentation of the computer code is contained in references [3],[4]. no further discussion of details of the code will be given here.

A description of the ISIS neutrino source and the modeling of the ISIS tungsten target will be provided in Sec. 2. Calculated neutrino fluxes from the spallation target and from the μSR target, and the background flux of $\overline{\nu}_e$ neutrinos are displayed in Sec. 3. The uncertainties in these neutrino fluxes are briefly discussed in Sec. 4. In Sec. 5 we compare measured and calculated absolute cross sections for a number of neutrino reactions on electrons and on atomic nuclei.

2 ISIS neutrino source

2.1 Time structure and energy spectra

It is the time structure in the ISIS proton beam that enables the physics of the KARMEN project to be separated into that initiated by ν_μ neutrinos or by ν_e and

$\overline{\nu}_\mu$ neutrinos. The proton beam consists of a pair of 100 ns wide pulses separated in time by 330 ns, within a 20 ms beam cycle.

The ν_μ neutrinos, with an energy of 29.8 MeV from the two-body π^+ decay at rest, have a time structure characteristic of the 26 ns pion mean life; the ν_e and $\overline{\nu}_\mu$ neutrinos, with the 0-53 MeV Michel spectral shapes from the three-body μ^+ decay, have the time structure of the 2.20 μs μ^+ mean life. This allows the separation (by timing) of the neutrinos produced from the pion decay, and from the subsequent muon decay. The energy spectra of the ν_μ neutrino from π^+ decay, and of the ν_e and $\overline{\nu}_\mu$ neutrinos from μ^+ decay, are shown in Fig. 1.

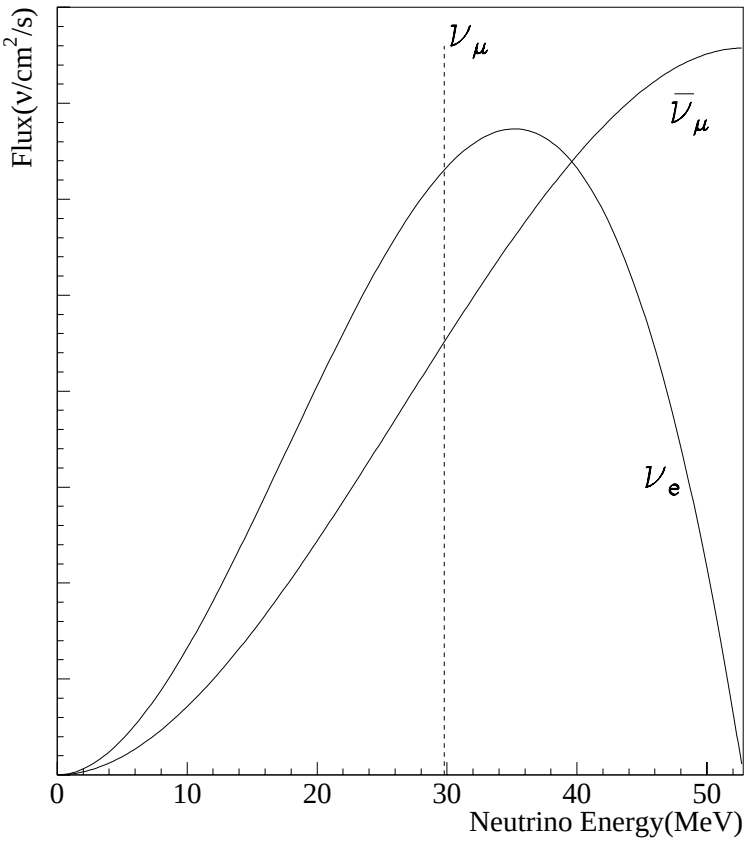

Figure 1: Energy spectra of the ν_μ neutrino from π^+ decay at rest, and of the ν_e and $\overline{\nu}_\mu$ neutrinos from μ^+ decay at rest.

2.2 ISIS spallation target

An overview of the input geometry model of the new ISIS tungsten spallation target is displayed in Fig. 2; for a similar picture of the tantalum model see ref.[3]. The 800 MeV proton beam, incident from the left in Fig. 1, first passes through a water-cooled Inconel beam window, then a helium filled void, and next through a tantalum

window entrance into the tungsten stack. It is stopped in a target, designed to produce spallation neutrons, consisting of layers of tungsten rectangular plates. Each tungsten plate is a rectangle of 80 mm X 105 mm, with thicknesses varying from 11 mm to 46 mm. In order to facilitate heat transfer, the tungsten plates are surrounded on all sides by tantalum structures in the form of headers, side plates, etc. Spaces between each plate assembly are filled with rapidly flowing heavy water as a coolant. The proton beam spatial distribution is a parabola 70 mm across, so that it is entirely contained within the area of the tungsten plates.

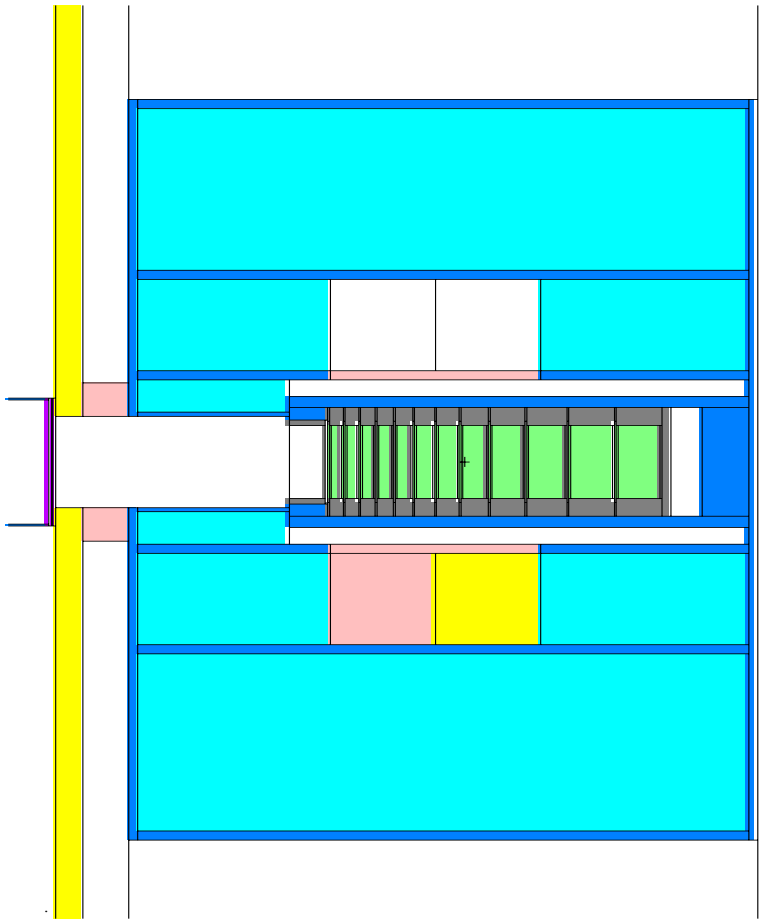

Figure 2: Geometry model of the ISIS tungsten spallation target assembly for input to the computer code. The proton beam is incident from the left; shown are the proton beam pipe, exit Inconel vacuum window, entrance collimator, tantalum window, and tungsten target structure. Above and below the tungsten target are four moderator cells.

The entire structure of plate assemblies is held within a stainless steel pressure vessel, containing manifolds for heavy water coolant. The geometry of the pressure vessel was

modelled with three layers of steel and three layers of water, in the plane transverse to that shown in Fig. 2. The total thickness of steel reproduces the volume of steel in the pressure vessel (excluding the top and bottom plates which could be modelled more exactly). A similar procedure was used for the water layers within the pressure vessel.

Surrounding the pressure vessel, as shown in Fig. 2, is the neutron reflector system, a vessel containing beryllium rods immersed in heavy water, and four neutron moderator cells. Between the beam windows and the reflector vessel, there is a beam halo monitor which is mounted on an aluminium flange. This was modelled as a circular ring 5cm thick, and was included because of its effect on the absorption of pions produced in the beam window.

3 Neutrino production from π^+ decay at rest

Input to the Monte Carlo code was provided by the ISIS spallation target model described in detail in Sec. 2.2 . For this geometry, all of the pion production and over 85% of the pion decays occur within the spallation target plate assembly. Only the small fraction of pions absorbed outside the plate assembly ($\sim 6\%$) is sensitive to the modelling of the pressure vessel. This region is, however, of more importance to the calculations of neutrino backgrounds from the π^- to μ^- decay chain.

Table 1: Calculated neutrino fluxes with the tantalum, uranium, tungsten and μSR targets for a proton beam energy of 800 MeV. Column 3 gives the neutrino production from μ^+ decay at rest in units of ν per proton, while column 4 gives the $\overline{\nu}_e$ background from μ^- decay at rest as a fraction of the number in column 3.

Spallation Target	Proton Energy (MeV)	Neutrino Flux ν_μ, ν_e, $\overline{\nu}_\mu$ (ν p^{-1})	Ratio $\overline{\nu}_e$ / ν_e (10^{-4})
Tantalum	800	0.0448	6.2
Uranium	800	0.0401	7.2
Tungsten	800	0.0425	4.5
μSR	800	0.0012	0.3

The decay-at-rest neutrino production, for target materials consisting of tantalum, uranium and tungsten, is given in Table 1. Results are expressed as the number of π^+ decays at rest per incident proton for the various target configurations. It is seen that the neutrino production from the new tungsten target will be approximately 95% of that from the tantalum target. This small reduction in the neutrno flux per incident proton will be only a small perturbation in any future neutrino program. Further, it should be noted that the ratio of $\overline{\nu}_e$ background to ν_e flux is significantly reduced, a result that

would be important for any future investigation of rare neutrino processes. A discussion of the $\overline{\nu}_e$ background listed in the last column of Table 1 will be given in Sec. 3.

3.1 Neutrino background from μ^- decay at rest

Virtually all π^- that stop are absorbed, and so the possible $\overline{\nu}_e$ backgrounds are created from the approximately 1% of the π^- that decay in flight. The μ^- from the decay in flight are tracked until they stop in some particular material; the fraction that leads to decay at rest rather than to absorbtion is calculated from measured muon total absorption rates[6] and is used to predict the $\overline{\nu}_e$ background. These fluxes, as a ratio to the ν_e flux, are shown in the last column of Table 1. From the entry in row 3, for a tungsten target and an 800 MeV proton beam, we get 0.18×10^{-4} $\overline{\nu}_e$ per incident proton.

The time structure in the ISIS proton beam, described in Sec. 2.1, enables this background to be substantially reduced. The time spectrum of $\overline{\nu}_e$ from the decay at rest of μ^- in the tungsten spallation source is shown in fig. 3. Here, the double-peaked initial shape is a consequence of the proton time struture, made up of two 100 ns wide pulses separated in time by 330 ns, with a repetition rate of 50 Hz. The total $\overline{\nu}_e$ time spectrum then consists of two basic components: (1) an exponential decay in low-Z materials Be and D_2O dominated by the 2.2 μs muon mean life, and (2) the much faster exponential decay in high-Z materials Fe, W and Ta characterized by a fast absorption rate.

Because the physics of the KARMEN experiment is normally separated into that due to ν_μ interactions (from the 26 ns π^+ decay at rest), and that due to ν_e and $\overline{\nu}_\mu$ interactions (from the 2.2 μs μ^+ decay at rest), events are separated into two time groups, above and below 600 ns from the start of the proton pulses. Inspection of Fig. 3 shows that 65% of the $\overline{\nu}_e$ are emitted after 600 ns, compared to 85% of the $\overline{\nu}_\mu$. Thus, *e.g.*, the expected experimental background to a neutrino oscillation search for the tungsten target would be reduced from 4.5×10^{-4} in the last column in Table 3 to a value $\overline{\nu}_e\ /\nu_e\ = 3.4\times10^{-4}$. It should be noted that the $\overline{\nu}_e$ background for the new tungsten target is 40% less than that for the tantalum target; this result could be important for any new program at ISIS that would study neutrino properties.

4 Neutrino flux uncertainty

Estimates of the uncertainties for the decay-at-rest neutrino fluxes from the ISIS tungsten spallation target are based upon the detailed error analysis for the decay-at-rest fluxes as discussed in ref[4]. There the absolute normalization of the code was provided by a mock beam stop experiment[5], LAMPF experiment E866. Error estimates for the new tungsten target are the same as those listed in ref.[3] for the KARMEN experiment, and are given here in Table 2. The measured pion production cross sections used in the Monte Carlo code typically have 9.5% absolute normalization errors. However, because

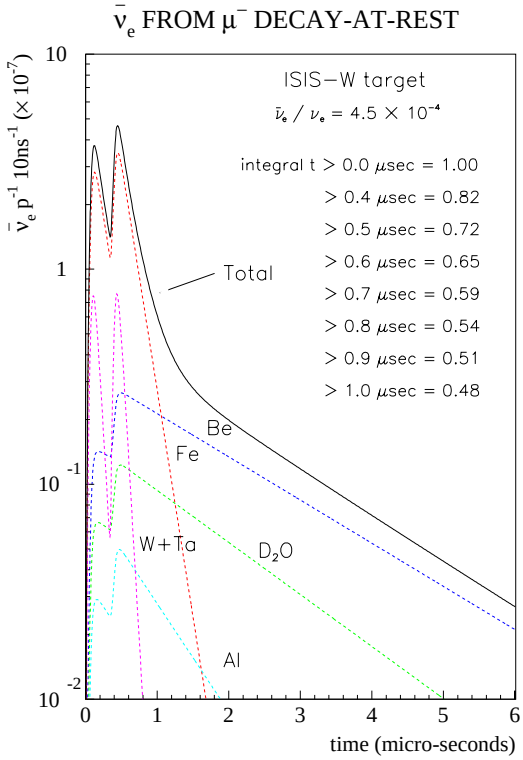

Figure 3: The time spectrum of $\overline{\nu}_e$ from the decay at rest of μ^- in the heavy water plus tungsten spallation target combination. The double-peaked initial shape is due to the proton time structure, while the total $\overline{\nu}_e$ time spectrum consists of two basic components, a relatively slow decay rate in low-Z materials (Be and D_2O) and the faster decay rate in high-Z materials (Fe, W and Ta).

the code was instead normalized to the E866 data on stopped π^+ per incident proton, this 9.5% uncertainty is irrelevant and is not included.

The sensitivity to the modelling of the geometry of the structures external to the spallation target and of the beam geometry were estimated in ref.[3] by making small changes in the appropriate spatial demensions.

For the central tungsten spallation target, calculations were performed for a series of succeedingly more accurate representations of the actual target construction. The changes in the calculated ν_e neutrino flux are listed in Table 3, where the first line lists the ν_e flux calculated for the ISIS tantalum target and discussed in ref.[3]. The model geometry "ISISA" is a first-approximation to the actual tungsten stack in the new target, and does represent most of the material changes in the central portion of the new tungsten target. In "ISISB" the heavy-water (D_2O) cooling channels on the

Table 2: Estimated errors in the calculated neutrino fluxes from π^+ decay at rest and μ^- decay at rest.

Source of uncertainty	π^+ Decay at rest (%)	μ^- Decay at rest (%)
Fit of E866 data	2.4	-
Cross section error	-	9.5
Systematic effects in E866	5.9	5.0
ISIS simulation	0.4	5.0
Proton beam energy	0.3	0.3
Protons on target	2.0	2.0
Proton geometry	0.6	0.6
Quadrature sum	6.7	12.0

sides of the tungsten stack are corrected; in "ISISC" the input window for the proton beam is changed from Inconel to tantalum; in "ISISD" the rear of the pressure vessel is appropriately modified; finally, in "ISISE" the exact definition is used for the tungsten and tantalum plates that make up each section of the central stack in the new tungsten spallation target. It can be seen from Table 3 that the changes in the ν_e flux are small, but still significant: the ν_e flux decreases by 3% in first going from tantalum to tungsten, and then decreases by another 2% as the model target geometry is refined. The small changes shown in Table 3, however, from "ISISC" to ISISE" do justify 0.4% for the entry in the line "ISIS simulation".

The main difference between the π^+ decay-at-rest and the μ^- decay-at-rest uncertainties in Table 2 occur in the absolute normalization. A normalization uncertainty for π^- decay in flight is composed of both a 9.5% contribution from the absolute normalization errors quoted in the pion production measurements, and a 5.0% contribution from the E866 experiment. This latter number comes from the part of the "systematic effects in E866" entry in Table 2 that represents a change in the code normalization, but that does not involve the pion production cross section errors.

In addition, a larger number (5.0%) is used for the ISIS simulation uncertainty in the π^- decay-in-flight flux because the moderator and shielding surrounding the target are not so well described as the elements of the central tungsten stack.

Table 3: Calculated neutrino fluxes for various stages of the input model geometry for the Monte Carlo computer program. The five model geometries represent changes in the tungsten spallation target and surrounding structure.

Model Geometry	Proton Energy (MeV)	Neutrino Flux ν_e (ν p^{-1})	Ratio
Tantalum	800	0.04480	1.000
ISISA	800	0.04350	0.971
ISISB	800	0.04346	0.970
ISISC	800	0.04258	0.950
ISISD	800	0.04251	0.949
ISISE	800	0.04249	0.948

5 Neutrino cross sections: comparison of measurement and calculation

A number of absolute neutrino cross section measurements, for a variety of reactions, have been made at the Rutherford-Appleton Laboratory (ISIS) and at the Los Alamos National Laboratory (LAMPF and LANSCE). At both laboratories, the neutrino fluxes produced from the interactions of the 800 MeV proton beams were calculated with the computer code mentioned in the Introduction. In this section we will compare the measured cross section values, which relie upon the neutrino flux computations, with theoretical cross section calculations.

The experiments include neutrino-electron scattering, charged- and neutral-current reactions on ^{12}C, charged-current inclusive reactions on ^{56}Fe, and charged-current reactions on ^{127}I to the bound states of ^{127}Xe. They are listed in Table 4 for the several experimental groups that have performed these measurements at the two laboratories.

For the LSND (ν_μ,μ^-) reactions the ν_μ beams were from pion decay-in-flight (DIF); for all the other reactions the neutrino beams were the 0-53 MeV ν_e and $\overline{\nu}_\mu$ beams, and the 30 MeV ν_μ beam, from pion and muon decay-at-rest (DAR). The measured and calculated cross sections, given in Table 4, have been averaged over the appropriate neutrino spectral shapes. For the listed experimental uncertainties, the first number is the statistical error and the second the systematic error. Errors in neutrino fluxes are included in the systematic part; as discussed in Sec. 4 and displayed in Table 2, the DIF beams have absolute uncertainties of 12% and the DAR beams absolute uncertainties of 6.7%. Although it is generally difficult to give errors for theoretical calculations, one can perhaps characterize the uncertainties in the values in the last column in Table 4 as ranging from less than 1% for $e^-(\nu_e,\nu_e)e^-$, to approximately 5% for $^{12}C(\nu_e,e^-)^{12}N_{gs}$, and to approximately 30% for $^{127}I(\nu_e,e^-)^{127}Xe_{bs}$.

Table 4: Comparison of measured and calculated cross sections for neutrino reactions. When there are two numbers for the listed experimental uncertainties, the first number is the statistical error and the second the systematic error.

Group	Spallation Target	Reaction	Measurement 10^{-42}cm^2	Calculation 10^{-42}cm^2
KARMEN	Ta	$^{12}C(\nu_e, e^-)^{12}N_{gs}$	$9.3 \pm 0.4 \pm 0.9$[7]	9.3[8]
		$^{12}C(\nu_e, e^-)^{12}N^*$	$5.1 \pm 0.6 \pm 0.5$ [7]	5.4[8]
		$^{12}C(\nu, \nu')^{12}C^*(15.1)$	$10.9 \pm 0.7 \pm 0.8$[7]	10.5[8]
		$^{56}Fe(\nu_e, e^-)X$	$256 \pm 108 \pm 43$[9]	273[10]
E225	H_2O, Al, Cu	$e^-(\nu_e, \nu_e)e^-$	$0.32 \pm .05 \pm .03$[11]	0.30
		$^{12}C(\nu_e, e^-)^{12}N_{gs}$	$10.5 \pm 1.0 \pm 1.0$[12]	9.3[8]
		$^{12}C(\nu_e, e^-)^{12}N^*$	3.6 ± 2.0 [12]	5.4[8]
LSND	H_2O, Al, W	$e^-(\nu_e, \nu_e)e^-$	$0.32 \pm .04 \pm .03$[13]	0.30
		$^{12}C(\nu_e, e^-)^{12}N_{gs}$	$8.9 \pm 0.3 \pm 0.9$[14]	9.3[8]
		$^{12}C(\nu_e, e^-)^{12}N^*$	$4.5 \pm 0.4 \pm 0.6$ [14]	5.4[8]
		$^{12}C(\nu_\mu, \mu^-)^{12}N_{gs}$	$58 \pm 8 \pm 10$[15]	64[16]
		$^{12}C(\nu_\mu, \mu^-)X$	$1020 \pm 44 \pm 180$[15]	1380[17]
E1213	H_2O, Al, Cu	$^{127}I(\nu_e, e^-)^{127}Xe_{bs}$	$254 \pm 80 \pm 14$[18]	260[19]

Inspection of Table 4 shows that all the measured cross section values are within one standard deviation of the calculated theoretical values. From column two in Table 4, we note that the neutrino production targets ranged from low-Z materials like H_2O and Al to high-Z materials like Ta and W. Since all the measurements relied upon the same computer code for their neutrino fluxes, the agreement between measured and calculated values strongly suggest that the neutrino flux computer code reproduces the actual neutrino fluxes remarkably well.

6 Summary

A Monte Carlo computer code, used for the calculation of neutrino fluxes from 800 MeV proton facilities, has been applied to the calculation of the neutrino fluxes to be expected from a new tungsten target at the ISIS spallation neutron source. The simulation of the tungsten spallation target was described in some detail. Results from application of the code, for ν_μ, ν_e, and $\overline{\nu}_\mu$ fluxes resulting from π^+ and μ^+ decay at rest,

were presented for tungsten, tantalum and uranium spallation targets and for a pyrolytic graphite μSR target for an incident proton beam of 800 MeV. An absolute accuracy of 6.7% on these neutrino fluxes was calculated from the normalization to a mock beam stop experiment.

The $\overline{\nu}_e$ backgrounds from the π^- decay-in-flight and subsequent μ^- decay-at-rest chain were also listed for the same target and proton beam combinations. The accuracy of these calculations was estimated to be 12% from a combination of the mock beam stop experiment and the uncertainties in the measured pion production cross sections. Use of the time structure of the proton beam at ISIS can reduce this background to a value $\overline{\nu}_e \ / \nu_e \ = 3.4 \times 10^{-4}$.

Measured values of cross sections for neutrino reactions, all of which utilized the Monte Carlo neutrino flux code of this report, were compared to theoretical calculations. The measured absolute cross sections are within one standard deviation of the theoretical calculations, and thus strongly support the accuracy of the Monte Carlo neutrino flux code.

7 Acknowledgements

We wish to acknowledge helpful conversations with T. Broome, G. H. Eaton, and M. Holding. This work was supported in part by the Forschungszentrum Karlsruhe (Germany) and by the Department of Energy (USA).

References

[1] B. Armbruster, *et al.*, Nucl. Phys. **B** (Proc. Suppl.) **38** (1995) 198; B. Armbruster, *et al.*, Nucl. Phys. **B** (Proc. Suppl.) **38** (1995) 235.

[2] B. Boardman, Rutherford Laboratory report, RL-82-006 (1982); for a current description, see http://www.isis.rl.ac.uk/

[3] R.L. Burman, A.C. Dodd and P. Plischke, Nucl. Instr. and Methods **A368** (1996) 416; R.L. Burman, A.C. Dodd and P. Plischke, Forschungszentrum Karlsruhe Report, FZKA 5595, July (1995). .

[4] R.L. Burman, M.E. Potter and E.S. Smith, Nucl. Instr. and Methods **A291** (1990) 621; R.L. Burman and E.S. Smith, Los Alamos National Laboratory report, LA-11502-MS (1989)

[5] R.C. Allen, *et al.*, Nucl. Instr. and Methods **A284** (1989) 347.

[6] T. Suzuki, D.F. Measday and J.P. Roalsvig, Phys. Rev. **C**35 (1987) 2212.

[7] R. Maschuw, *et al.*, Prog. Part. Nucl. Phys. 40, (1998) 183, Ed. A. Faessler (Elsevier Oxford).

[8] E. Kolbe, *et al.*, Phys. Rev. **C**49 (1994) 1122; E. Kolbe, K. Langanke and P. Vogel, Nucl. Phys. **A652** (1999) 91.

[9] C. Ruf, PhD thesis, University of Bonn (1999).

[10] E. Kolbe, K. Langanke and G. Martínez-pinedo, nucl-th/9905001 (1999).

[11] R.C. Allen, *et al.*, Phys. Rev. **D**47 (1993) 11.

[12] D.A. Krakauer, *et al.*, Phys. Rev. **C**45 (1992) 2450.

[13] L.B. Auerbach, *et al.*, Phys. Rev. **D**63 (2001) 112001.

[14] L.B. Auerbach, *et al.*, hep-ex/0105068 (2001) submitted to Phys. Rev **C**.

[15] L.B. Auerbach, *et al.*, to be submitted to Phys. Rev **C**; C. Athanassopoulos, *et al.*, Phys. Rev. **C**56 (1997) 2806; R. Imlay, *et al.*, Nucl. Phys. **A629**, (1998) 531c.

[16] J. Engel, *et al.*, Phys. Rev. **C**54 (1996) 2740.

[17] A.C. Hayes and I.S. Towner, Phys. Rev. **C**62 (2000) 044603.

[18] J.R. Distel, *et al.*, to be submitted to Phys. Rev. **C**.

[19] J. Engel, S. Pittel and P. Vogel, Phys. Rev. **C**50 (1994) 1702; the cross section value quoted in Table 4 is an average of calculations for free and quenched values of the axial current g_A.